Recycling Ambient Radiofrequency (RF) Energy: Far-Field Wireless Power Transfer and Harmonic Backscattering

Xiaoqiang Gu, Pascal Burasa, Simon Hemour, Ke Wu

▶ **To cite this version:**

Xiaoqiang Gu, Pascal Burasa, Simon Hemour, Ke Wu. Recycling Ambient Radiofrequency (RF) Energy: Far-Field Wireless Power Transfer and Harmonic Backscattering. IEEE Microwave Magazine, 2021, 22 (9), pp.60-78. 10.1109/MMM.2021.3086335 . hal-04559908

HAL Id: hal-04559908
https://hal.science/hal-04559908v1

Submitted on 25 Apr 2024

HAL is a multi-disciplinary open access archive for the deposit and dissemination of scientific research documents, whether they are published or not. The documents may come from teaching and research institutions in France or abroad, or from public or private research centers.

L'archive ouverte pluridisciplinaire **HAL**, est destinée au dépôt et à la diffusion de documents scientifiques de niveau recherche, publiés ou non, émanant des établissements d'enseignement et de recherche français ou étrangers, des laboratoires publics ou privés.

Recycling Ambient Radiofrequency (RF) Energy: Far-Field Wireless Power Transfer and Harmonic Backscattering

Xiaoqiang Gu[1], Pascal Burasa[1], Simon Hemour[2], and Ke Wu[1]

[1]Poly-GRAMES Research Center, Polytechnique Montreal, Canada

[2]IMS Laboratory, CNRS UMR 5218, Bordeaux INP, University of Bordeaux, France

It all started with a spark. Let us rewind back to 1887, in Germany. The days were getting cooler in the garden of the Technische Hochschule in Karlsruhe as Heinrich Rudolf Hertz was setting up the first-ever far-field wireless power transmission with increasingly more power [1]. He was striving to demonstrate the wireless nature of electromagnetic waves and propagation. Moreover, since no high frequency (nearly 100 MHz) voltmeter was available at that time for his experiment, he had to transmit enough power to generate a spark —hundreds of volts!— at the receiver to validate the famous theory of James Clerk Maxwell.

Since this first experimental verification, radiofrequency (RF) wave-based wireless technology has seen rapid developments in many different directions. So far, two primary system functions of wireless technology, namely wireless communication and wireless sensing, have already become the foundations of our modern social and economic life for ubiquitous connectivity, social networking, and environmental awareness [2]. Ambient RF waves quietly flow all around us from radio and digital TV broadcasting towers, cellular stations, Wi-Fi access points to support wireless communication and sensing applications. Besides what is consumed by end-users, a significant portion of ambient RF waves decay in free space and is finally wasted. Therefore, the topic of recycling ambient RF energy whenever and wherever possible has recently emerged and amassed vast attention [3-5]. Ambient RF energy is highly suitable as external ready-to-use power sources for ultra-low-power internet of things (IoT) sensors. In the coming future, IoT sensors will be scattered everywhere in our environment, thus making power cords or battery-based solutions costly and inadequate. Moreover, many IoT sensors, such as temperature and CO_2 monitoring elements, do not need a continuous operation, thereby suggesting they are less power-hungry. Harnessing ambient RF energy can

fundamentally unlock ubiquitous remote sensing's potential as the two dimensions of geographical distribution and power supply/consumption no longer draw obstacles. Hence, despite relatively low power density, omnipresent ambient RF power is an ideal, green power source for ultra-low-power IoT sensors.

Power Density of Ambient RF Energy in Urban and Suburban Areas

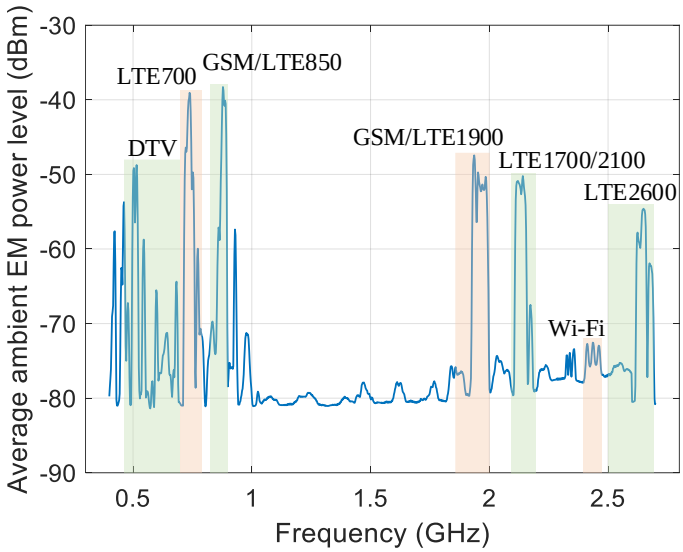

(a)

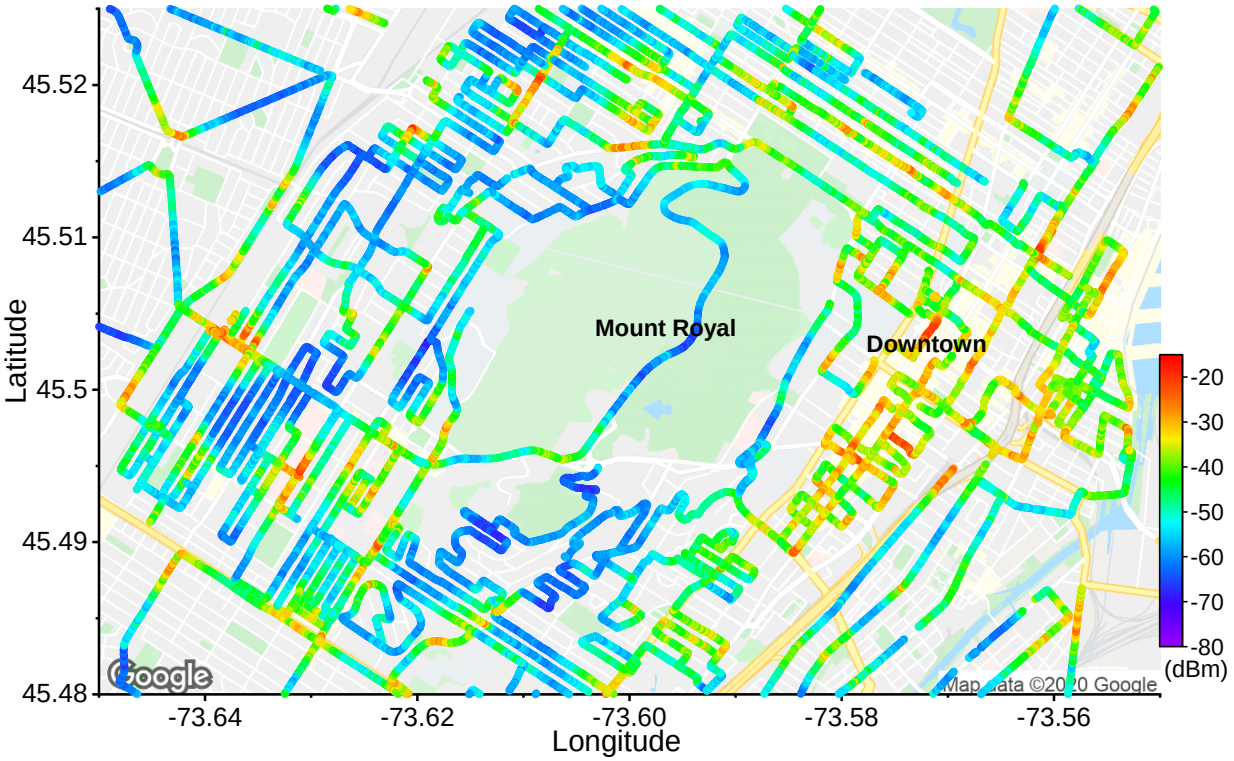

(b)

Figure 1. (a) Average RF power density in Downtown Montreal across the frequency spectrum of 400 MHz to 2700 MHz. (b) Dynamic measurement results of ambient RF power (GSM/LTE850 band) in core areas of Montreal, Canada.

Before jumping into the design process, knowing how much ambient RF energy is available in our daily environment must be the very first step. This will validate the next steps in development. With the roll-out of 5G, more ambient RF power will emerge at higher frequency bands [6]. Nevertheless, the sub-7 GHz frequency band is still the best choice for recycling ambient RF energy in considering its low transmission loss, high-level signal coverage, and abundantly available frequencies. Based on frequency allocation charts, the sub-7 GHz frequency band can be further categorized into seven primary groups, namely DTV, LTE700, GSM/LTE850, LTE1700/2100, GSM/LTE1900, Wi-Fi, and LTE2600 bands. Note that the ambient RF power below the DTV band, such as FM radio, is not included since the recycling circuit/system size will be problematically large for IoT sensor nodes in such low frequencies.

So far, multiple investigations on ambient RF power density in the sub-7 GHz band were carried out in different cities across the world [7-9]. Such measurements usually target fixed locations close to places involving substantial pedestrian traffics. To cover a larger geographical area and reflecting more representative conditions, the dynamic outdoor mapping of ambient RF energy in the city of Montreal was reported in [10]. Ambient RF power density was measured and evaluated along streets, roads, avenues, and highways—a contrast from previous stationary/fixed-location measurements. Figure 1 (a) illustrates the average ambient RF power density levels over the frequency band of interest (400 MHz ~ 2700 MHz) in Downtown Montreal, Canada [10]. Among the above seven sub-7 GHz frequency bands, the GSM/LTE850 band shows the largest average ambient RF power level (−38.29 dBm). Next to the GSM/LTE850 band, the LTE700 band has a comparable average power level of −39.05 dBm. Moreover, the DTV and GSM/LTE1900 bands also have a similar level of average RF power density, slightly higher than −50 dBm. Figure 1 (b) presents the dynamic measurement results of ambient RF power density (GSM/LTE850 band) in the core areas of Montreal. It can be clearly observed that Downtown Montreal has a higher overall ambient RF power density than the other areas. The highest recorded power level is about −13 dBm. Based

on the above measurement results and discussions, the circuit/system design aiming to recycle ambient RF power should target a power level of −15 dBm and below. The actual amount of power harvesting depends on many factors, including the effective antenna aperture.

Two Main Techniques: Far-field Wireless Power Transfer (WPT) and Harmonic Backscattering

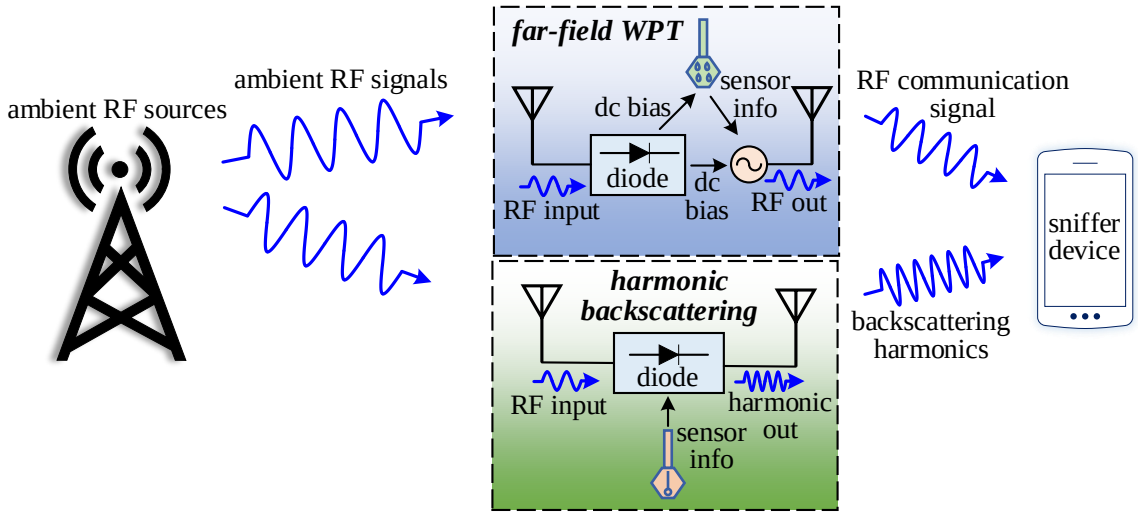

Figure 2. Far-field wireless power transfer (WPT) and harmonic backscattering are two mainstream technologies for recycling ambient RF energy in free space.

Currently, recycling ambient RF energy can be mainly realized by two types of techniques: far-field wireless power transfer (WPT) and harmonic backscattering, as shown in Figure 2. Ambient RF energy is in both cases collected by the antennas and injected into a nonlinear device for frequency conversion. The primary difference between these two techniques lies in the frequency components after conversion. Far-field WPT converts the RF energy input into dc power, which is then used to drive sensing and communication operation with sniffer devices [11], [12]. By contrast, harmonic backscattering up-converts RF input into higher harmonics, in most cases the second harmonic [13], and directly uploads information to sniffer devices [14], [15].

Both techniques have recently gained increasing attention in the microwave community, which is revealed in Figure 3. For example, Figure 3 (a) shows the number of papers appearing in two major

databases, Web of Science and IEEE Xplore, when the search hits wireless power transfer as author keywords. To further identify works in the particular domain of far-field WPT, the keywords "far-field/RF/radiative" have been introduced to refine results within the initial search outcome. In Figure 3 (a), the total number of papers on WPT has been continuously growing since 2010 in both databases. Noticeably, a big jump in papers occurred in the year 2015. Moreover, the far-field WPT papers account for roughly 10 % ~ 15 % of the total number of papers in the research field of WPT. As a new topic, the far-field WPT has become more and more attractive since the last decade and, currently, turns out to be an intriguing, trendy field.

Figure 3 (b) presents the search results for "wireless/RF/radiofrequency/microwave backscatter" or "harmonic tag/transponder/backscatter" as author keywords in both databases. The total number of papers in both databases shows an increasing trend since the year 2010, although this number is smaller compared to that of the WPT domain. When further refining the search results by using "harmonic" as a keyword, the number of filtered papers is small without a clear increasing trend, indicating this research topic is relatively new and may hold much potential.

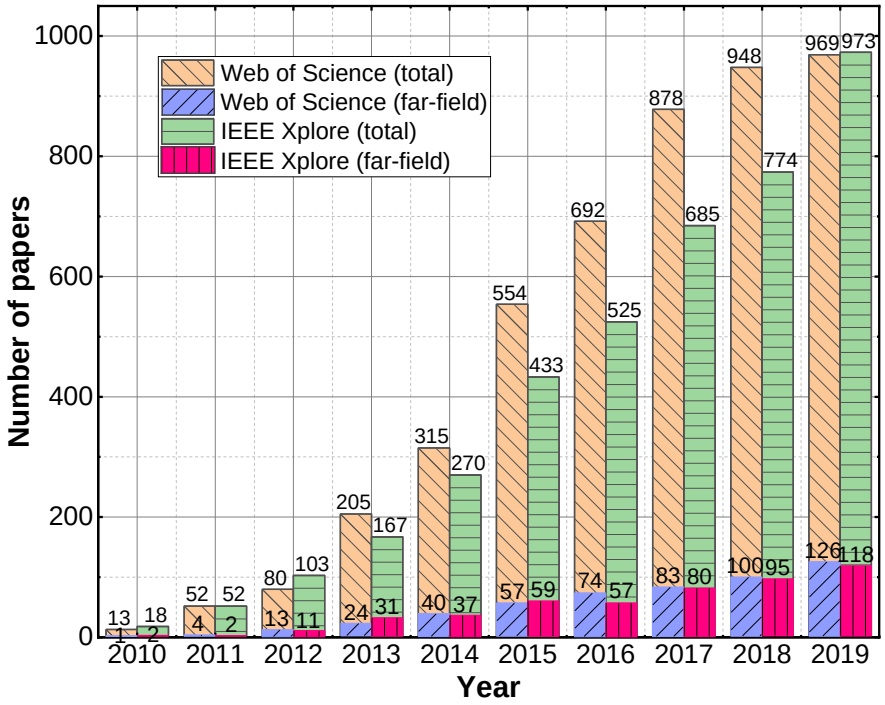

(a)

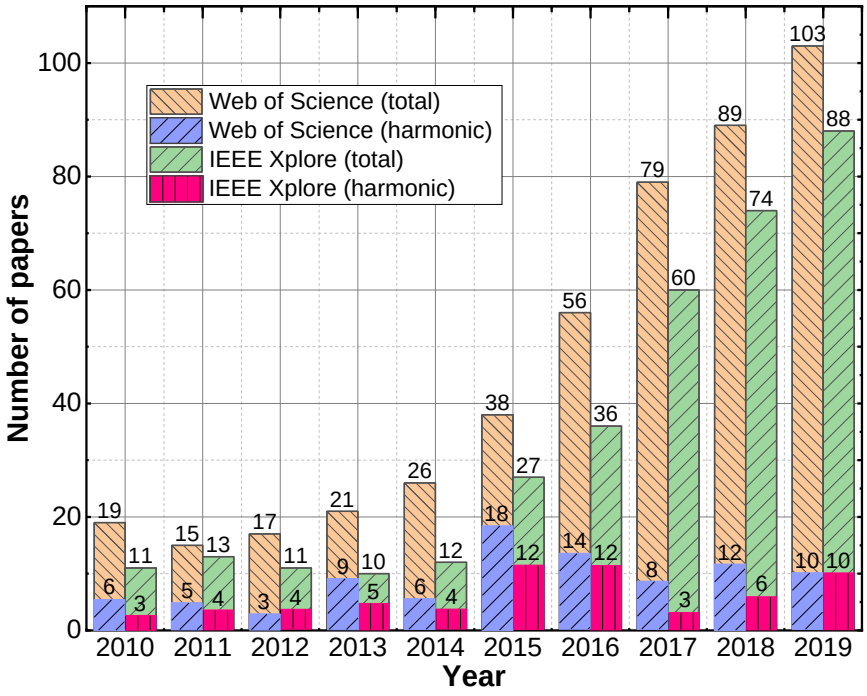

(b)

Figure 3. Number of papers in the last decade (2010 ~ 2019) in the research domain of WPT and backscattering. The papers of far-field WPT and harmonic backscattering are further filtered out in the corresponding research fields. Results reveal the outcome of author keywords search in Web of Science and IEEE Xplore. (a) WPT and far-field WPT; (b) Wireless/RF/radiofrequency/microwave backscattering and harmonic backscattering.

Featuring low cost, a well-established fabrication process, and easy accessibility, commercial Schottky diodes working as a nonlinear device for recycling ambient RF energy are still the top choice and will be the focus in this work. Frequency conversion is realized by diode nonlinearity, which indicates that the output signal does not have a linear response to the input. The nonlinearity of Schottky diodes contains two contributors, namely, the junction resistance and junction capacitance. Far-field WPT relies on the nonlinear junction resistance, while harmonic backscattering depends on the nonlinear junction resistance and capacitance simultaneously, which will be discussed in detail later. As mentioned before, the primary difference between far-field WPT and harmonic backscattering lies in how designers select and maximize the target frequency components. As depicted in Figure 4, the *I-V* curve of a typical Schottky diode reflects

its nonlinearity. Assuming a sinusoidal RF signal travels through this diode, its output would consist of the fundamental signal, dc component, second harmonic, and other higher harmonics. Getting the most of the dc component and second harmonic at the output ports is the design goal of far-field WPT and harmonic backscattering circuits/systems, respectively. All design efforts are to maximize the outcome of target frequency components; in other words, to suppress the energy outputs at other frequencies.

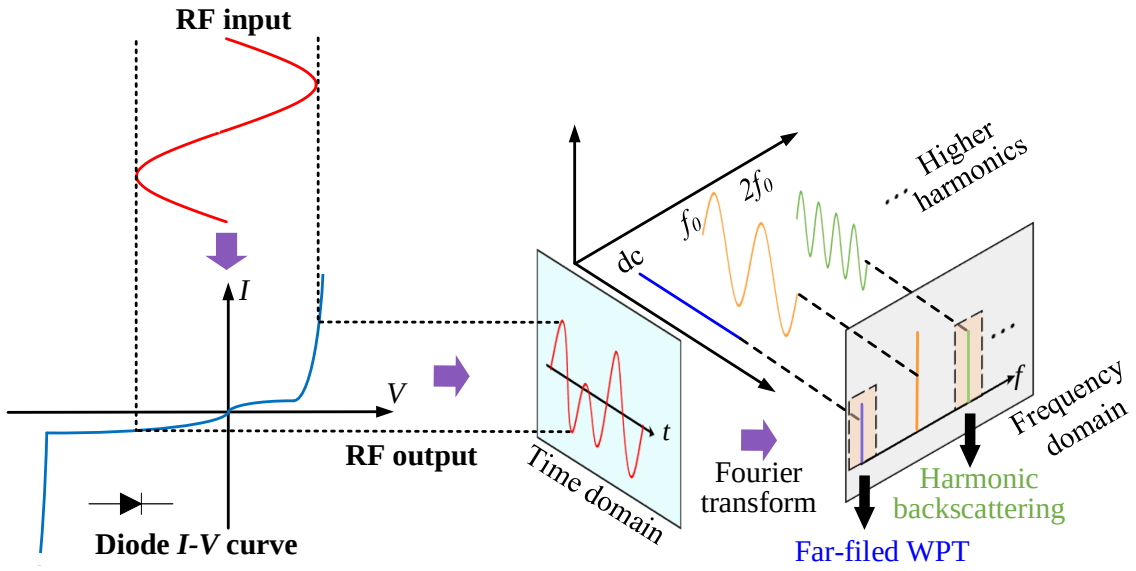

Figure 4. Diode nonlinearity would generate all frequency components with a sinusoidal RF input. Far-field WPT and harmonic backscattering circuits/systems maximize the output of dc component and second harmonic, respectively.

Current responsivity $\Re_I$ is often used to quantify the nonlinearity of diodes in RF-to-dc frequency conversion [16]. It is defined as the ratio of dc short-circuit current I_{dc} over RF input power P_{in} [17]:

$$\Re_I = \frac{I_{dc}}{P_{in}} \tag{1}$$

When the RF input power is low, which indicates the Schottky diode works in the square law region, the current responsivity $\Re_I$ can be simplified as the quadratic responsivity $\Re_{I0}$. For a Schottky diode, this value can be calculated by its SPICE parameters on the datasheets offered by manufacturers [18]:

$$\Re_{I0} = \frac{q}{2n \cdot k \cdot T} \tag{2}$$

where q, n, k, and T are the electron charge, diode ideality factor, Boltzmann constant, and operation temperature (in Kelvin), respectively. The current responsivity of diodes is a significant quantitative indicator associated with the efficiency performance of both far-field WPT and harmonic backscattering.

Analysis of Diode-Based Far-Field WPT Rectifiers

Considering that the available ambient RF power is relatively low in free space, the circuit topology of far-field WPT rectifiers based on a single diode will lead to higher efficiency. Furthermore, the topologies based on single-shunt and single-series diodes illustrate a negligible difference in rectifying efficiency, despite having different dc paths. Thus, the single-series topology with fewer lumped components is selected for discussion in this work. Figure 5 shows the equivalent circuits of single-series rectifier analysis. The Schottky diode is characterized by the well-known Shockley model [19], which consists of nonlinear junction resistance R_j, nonlinear junction capacitance C_j, series resistance R_s, parasitic capacitance C_p and inductance L_p. The equivalent circuit in Figure 5 (a) shows a state where the diode absorbs injecting RF power. Inside the diode junction, both nonlinear junction resistance R_j and capacitance C_j convert the fundamental RF signal into other frequency components. However, due to the nature of dc output—it cannot go through junction capacitance C_j—only nonlinear junction resistance R_j contributes to the frequency conversion in far-field WPT rectifiers. The nonlinear junction capacitance C_j is an indirect power dissipator, and the RF input power passing through it is eventually dissipated by the series resistance R_s. After frequency conversion, the diode acts as a dc power source for the load resistance R_l, which is represented by the equivalent circuit in Figure 5 (b).

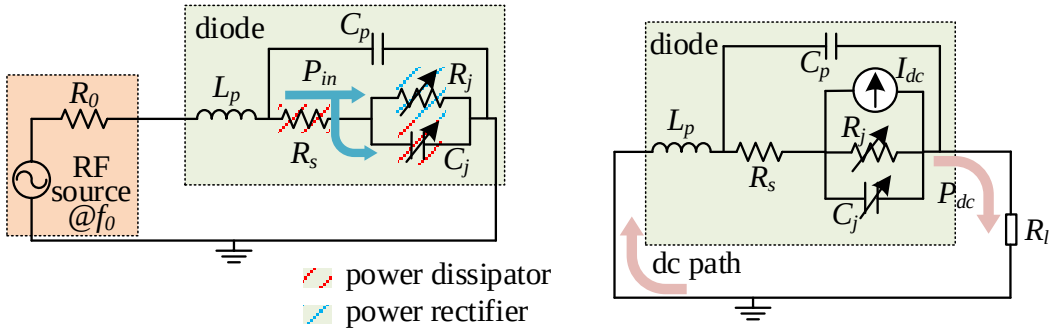

(a) (b)

Figure 5. Equivalent circuits of diode operations in the rectifier before and after frequency conversion: (a) diode absorbing RF input power and (b) diode serving as a dc power generator.

Based on the equivalent circuit analysis in Figure 5, the rectifier efficiency η_{re} can be calculated by [17, 18, 20]:

$$\eta_{re} = \eta_d \cdot \eta_p \cdot \eta_t = \frac{P_{in} \cdot \Re_I^2 \cdot R_j^2}{R_l + R_s + R_j} \cdot \left(\frac{1}{1 + (\omega \cdot C_j)^2 \cdot R_s \cdot R_j} \right)^2 \cdot \frac{R_l}{R_l + R_s + R_j} \tag{3}$$

where η_d, η_p, η_t are the rectifying efficiency of the diode junction resistance, parasitic efficiency (due to junction capacitance), and dc power transfer efficiency, respectively. ω is angular frequency. This explicit expression of efficiency prediction is a guideline to optimize the design of far-field WPT rectifiers:

a. Select suitable Schottky diodes;

b. Enhance input power level P_{in}; and

c. Optimize load resistance R_l.

A. Diode Selection for Far-Field WPT Rectifiers

Based on the efficiency calculation in (3), several rules for diode selection can help to quickly identify suitable candidates: preferred diodes are paired with (a) stronger nonlinearity, or in other words, higher current responsivity $\Re_I$; (b) larger nonlinear junction resistance R_j or smaller saturation current I_s; (c) smaller nonlinear junction capacitance C_j and series resistance R_s. Beyond these simple rules applicable to easy cases, an accurate calculation method or simulation is often required to evaluate diode candidates thoroughly.

Table I lists popular commercial diodes for recycling ambient RF energy for both far-field WPT and harmonic backscattering applications. The main SPICE parameters and zero bias current responsivity $\Re_{I0}$ of those diodes are also attached for analysis. Regarding the four diodes for far-field WPT rectifiers in Table I, Figure 6 presents the rectifying efficiency and dc output voltage results obtained through the harmonic balance simulator of the Advanced Design System (ADS) software. The load resistance R_l for each diode is optimized at a reasonable power level of −20 dBm according to the ambient RF power density study discussed before. The operating frequency is 880 MHz, corresponding to the frequency point with the highest average ambient RF power density in Figure 1 (a).

Table I SPICE parameters and $\Re_{I0}$ of popular diodes for recycling ambient RF power

Far-field WPT

	HSMS-282x	HSMS-286x	SMS7630	HSMS-285x	HMPS-2820	SMV1430
I_s (A)	2.2e-8	5e-8	5e-6	3e-6	2.2e-8	1e-14
R_s (Ω)	6	6	20	25	8	3.15
n	1.08	1.08	1.05	1.06	1.08	1
C_{j0} (pF)	0.7	0.18	0.14	0.18	0.7	1.11
M	0.5	0.5	0.4	0.5	0.5	0.5
F_c	0.5	0.5	0.5	0.5	0.5	0.5
V_j (V)	0.65	0.65	0.34	0.35	0.65	0.86
B_V (V)	15	7	2	3.8	15	0
I_{BV} (A)	1e-4	1e-5	1e-4	3e-4	1e-4	1e-3
$\Re_{I0}$ (A/W)	18.02	18.02	18.53	18.36	18.02	19.46

harmonic backscattering

Figure 6 indicates that HSMS-286x is a better choice for rectifier design since its rectifying efficiency and dc output voltage are the highest among the four diodes in the power range of interest. Its rectifying efficiency is at least 10 % and 8 % higher than the rest at −30 dBm and −20 dBm, respectively. Noticeably, the dc output voltage of HSMS-286x is close to 0.7 V at −20 dBm. It is more than two times greater than the second-highest at the same power level, referring to SMS7630's approximate 0.3 V. Moreover, the diode HSMS-286x has a breakdown power level of −8 dBm, which is enough for the ambient

RF energy recycling applications. It should be noted that the breakdown power level of each diode varies with its load resistance. Thus, a careful evaluation is recommended for each design scenario.

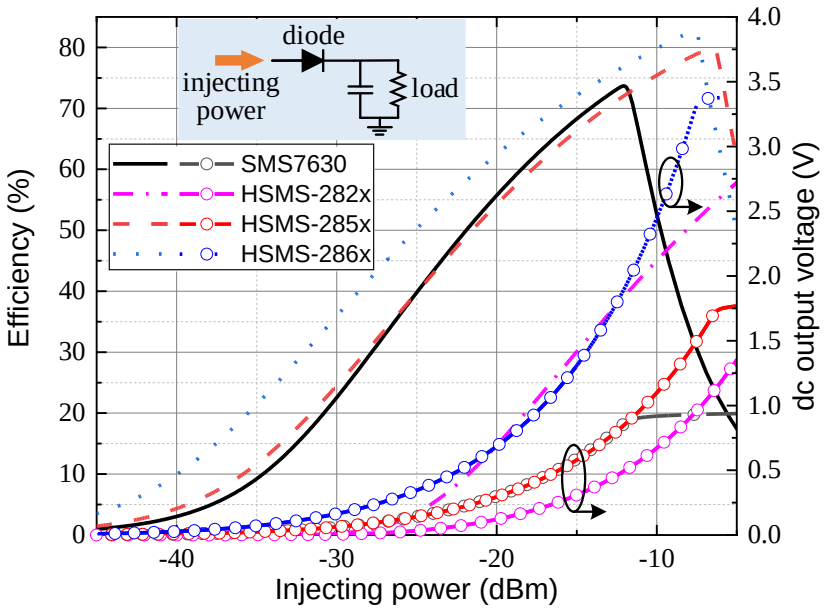

Figure 6. Rectifying efficiency and dc output voltage of four selected diodes for far-field WPT rectifiers (Table I) when utilized in a single-series topology. Optimized load resistances for peak efficiency at −20 dBm are 16 kΩ for SMS7630 and HSMS-285x, 75 kΩ for HSMS-286x, and 10 kΩ for HSMS-282x.

Since diodes SMS7630 and HSMS-285x share similar SPICE parameters, as listed in Table I, both diodes present similar responses in rectifying efficiency and dc output voltage, as shown in Figure 6. The rectifying efficiency is roughly 24 % and 66 % at −30 dBm and −15 dBm, respectively, for both diodes. The main difference between these two diodes is the breakdown voltage, where HSMS-285x obtains a higher breakdown power level (−6.5 dBm). Thus, its dc output voltage of 1.7 V saturates at a higher level than that of the 0.9 V belonging to SMS7630. As for the diode HSMS-282x, its rectifying efficiency in the power range of interest is not satisfactory. Nevertheless, with a higher breakdown voltage, HSMS-282x is suitable for high-power rectifier design as rectifying efficiency begins to steadily increase when injecting power exceeds −10 dBm.

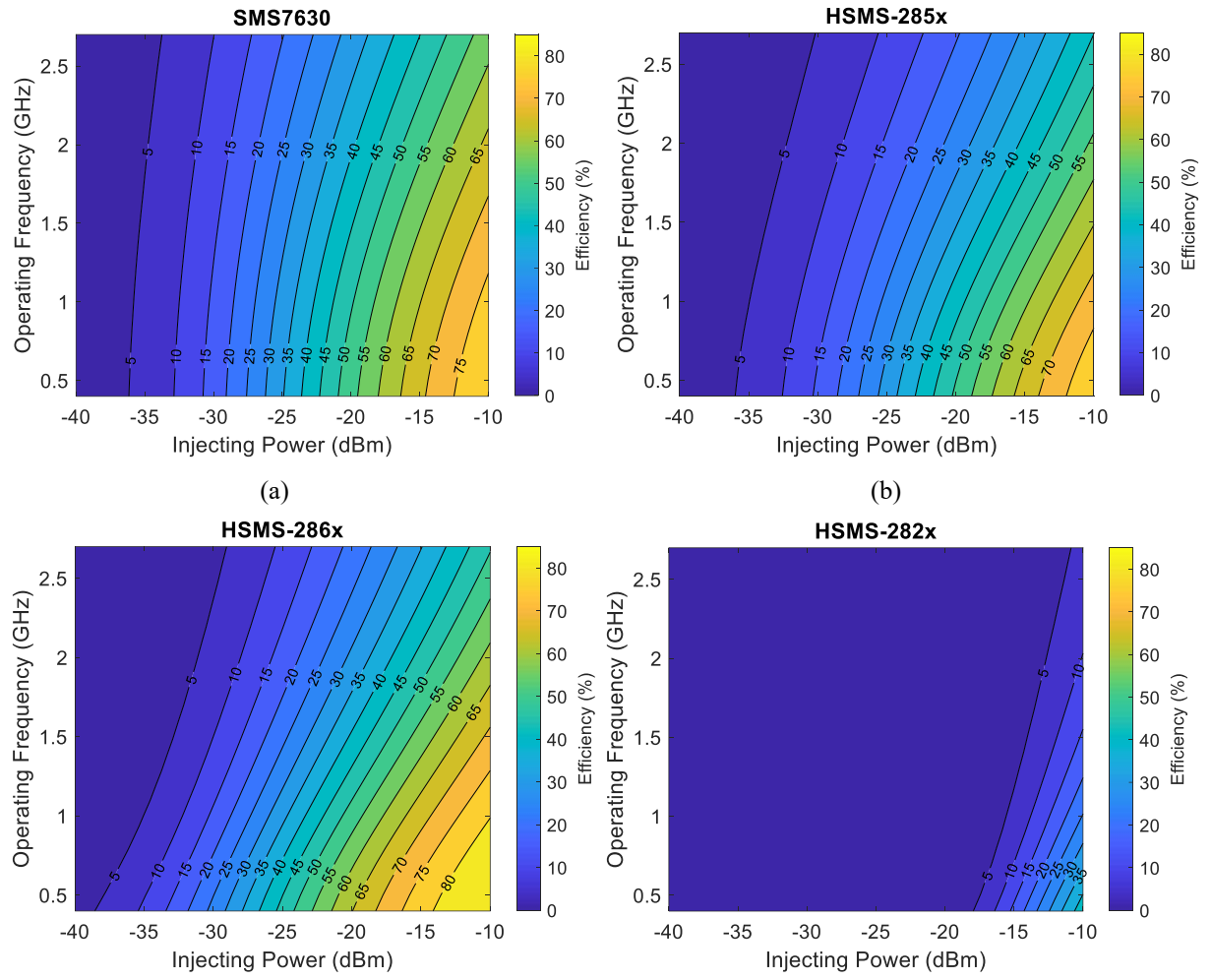

Figure 7. Calculated rectifying efficiency of four selected diodes against injecting power (−40 dBm to −10 dBm) and operating frequency (0.4 GHz to 2.7 GHz). Load resistances for each diode are the same as in Figure 6. Each subplot contains efficiency contours. (a): SMS7630; (b): HSMS-285x; (c): HSMS-286x; and (d): HSMS-282x.

The operating frequency of diodes also plays a significant role in their rectifying efficiency. Hence, Figure 7 attempts to reveal the rectifying efficiency performance of the selected four diodes as a function of injecting power and operating frequency simultaneously. The above results are calculated through the efficiency prediction method reported in [21]. According to the aforementioned equivalent circuit analysis, as the only contributor to frequency conversion in rectifiers, junction resistance R_j is not frequency-dependent. However, part of the injecting power goes around through the frequency-dependent junction

capacitance C_j and are eventually dissipated. Thus, the diode parasitic efficiency due to the junction capacitance C_j varies with operating frequency as seen in Figure 7. With a larger C_j, the diode rectifying effiency would decline at a faster rate with an increasing operating frequency. Such a claim can be verified in the comparison between diodes HSMS-286x (C_{j0} = 0.18 pF) and SMS7630 (C_{j0} = 0.14 pF) in Figure 7 (a) and (c), respectively. For example, with the input power of −25 dBm, the calculated rectifying efficiency of HSMS-286x is 46.87 % versus 34.65 % of SMS7630 at 400 MHz. When the operating frequency increases to 2700 MHz, the rectifying efficiency of HSMS-286x reduces to 10.95 %, while SMS7630 still obtains an efficiency of 19.77 %. As seen in Figure 7 (a) and (b), the diodes SMS7630 and HSMS-285x have similar patterns of rectifying efficiency. Due to a slightly larger junction capacitance C_j, the decreasing rate in rectifying efficiency of HSMS-285x against an increasing operating frequency is larger than that of SMS7630. Figure 7 (d) verifies that HSMS-282x is suitable for high-power rectifier applications. Through this investigation, it reveals that SMS7630 is the top choice for far-field WPT rectifier design when the operating frequency goes beyond roughly 1.5 GHz.

B. Input Power Enhancement

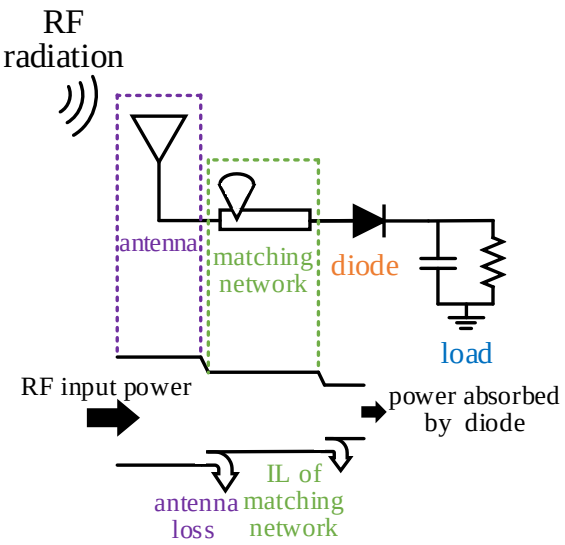

Figure 8. Careful design of antenna and matching networks enhances total power absorbed by the diode, finally leading to higher rectifying efficiency.

As shown in Figure 6, the rectifying efficiency of diodes ramps up with higher injecting power. Thus, the preceding stages in rectifier design, namely antenna and impedance matching network (Figure 8), must be optimized to minimize potential insertion loss. For antenna design, maximizing antenna efficiency entails harnessing the ambient RF energy in free space as much as possible. Multi-band rectennas (rectifying antenna), which can scavenge ambient RF power in multiple bands, are highly desirable [22-25]. As an example, Figure 9 (a) illustrates a triple-band rectenna, which covers the frequency bands 0.79 GHz – 0.96 GHz, 1.71 GHz – 2.17 GHz, and 2.5 GHz – 2.69 GHz [22]. Such a triple-band rectenna has already covered major sub-7 GHz communication bands. Besides multi-band rectennas, utilizing an antenna array is a straightforward way to acquire more ambient RF power. It increases the effective antenna aperture since the receiving power of an antenna directly depends on its physical size [26, 27]. However, as the array inevitably occupies more space, it is only suitable when enough room is available for the rectenna. Furthermore, high gain antennas are also preferred in rectenna design to enhance diode rectifying efficiency thanks to a larger input power level. Nevertheless, the broad angular coverage and high gain of a single-element antenna contradict each other. For example, omnidirectional dipole rectennas featuring quasi full spatial coverage are often the first choice to scavenge incoming RF power from various directions. However, the low gains of omnidirectional dipole antennas cannot support an efficient rectifying process inside the rectennas. To overcome this problem, a well-organized scheme of a high-gain antenna array to target ambient RF power in each direction is an intriguing solution shown in Figure 9 (b) [28]. Such an idea whereby an array is used to extend the far-field WPT rectifying coverage has been extensively investigated, as it breaks the contradiction of high gain and broad spatial coverage set by one single-element antenna [29-31].

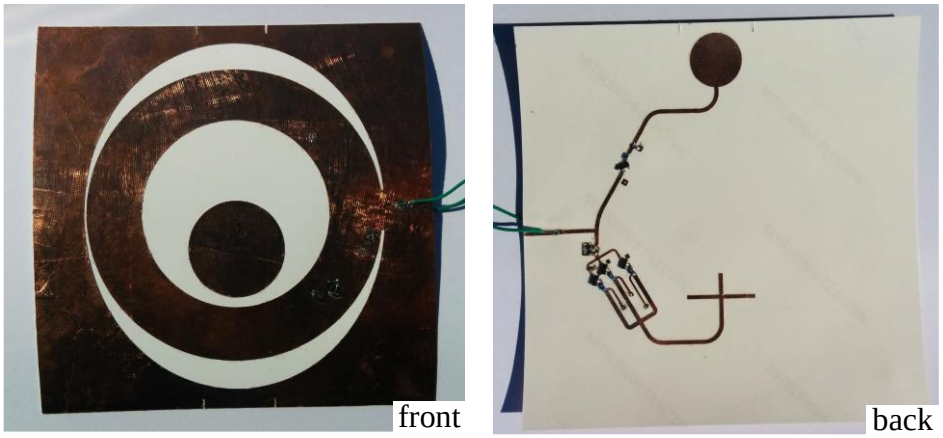

(a)

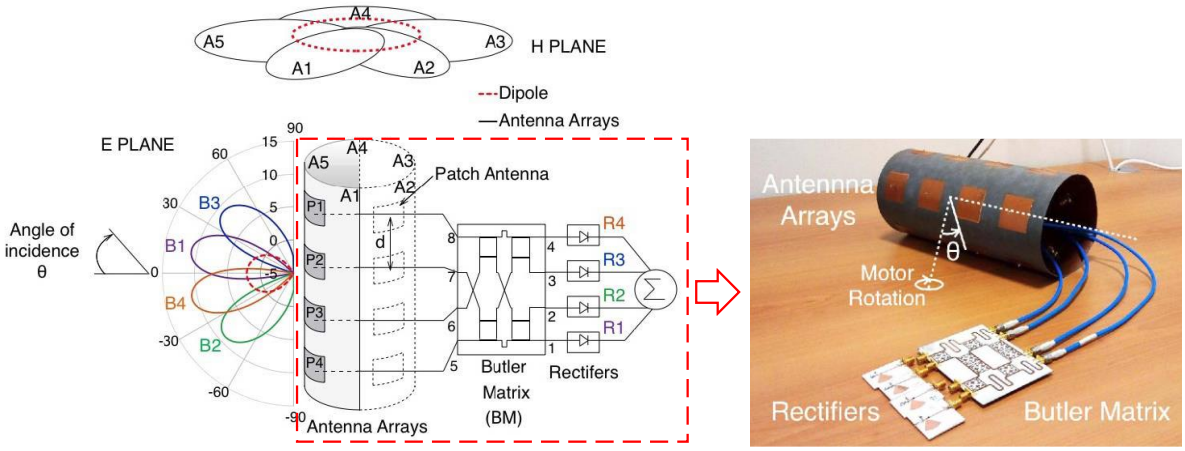

(b)

Figure 9. (a) Triple-band rectenna reported in [22]. (b) Rectenna with an optimal angular coverage [28].

Besides pervasive ambient RF power, ample vibration, thermal, and solar energy exist in our environment [11]. Cooperatively harvesting two or more of the above energy sources is an efficient way to generate more dc output. Due to different transduction mechanisms, vibration energy is generally converted into low-frequency AC signals first [32]. In contrast, the output of thermal and solar energy conversion is dc power, which does not need any further frequency conversion [33],[34]. Hence, cooperatively collecting from multi-physical sources requires different strategies for power combinations [35]. For hybrid RF and vibration energy harvesting, it is better to inject two power sources into the rectifying diode simultaneously, as seen in Figure 10 (a). Measurement results of hybrid energy harvesting show that enhanced total dc output power has been obtained, compared with the simple superposition of a separate energy harvesting

method [36]. By contrast, for thermal/solar energy, combining the rectified dc output power of ambient RF and thermal/solar energy on the load resistance is a more economical way. Figure 10 (b) presents an example of a hybrid solar and RF energy rectifier based on flexible substrates [34].

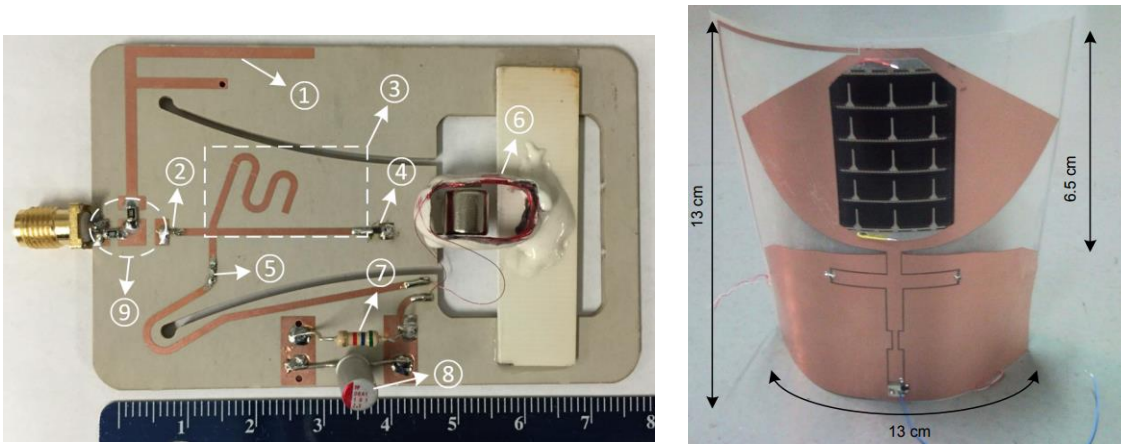

(a) (b)

Figure. 10. (a) Prototypical hybrid RF and vibration energy harvester [36]; (b) Flexible substrate-based hybrid solar and RF energy rectifier [34].

The matching network placed between a receiving antenna and a diode accomplishes impedance transform to maximize power transfer. For a given nonlinear device, the performance of the matching network makes a big difference for the entire rectifying efficiency, as shown in Figure 11 (a). Typically, antennas are designed to have a standard 50-Ω impedance. Whereas, Schottky diodes often reflect a high impedance when input power is relatively low. The matching network efficiency η_m can be defined as the power reaching the diode divided by the RF power received by the antenna. And if the Q factor is introduced, η_m can be written as:

$$\eta_m = \frac{1}{1+\frac{Q_r}{Q_m}} = \frac{1}{1+\frac{\sqrt{\frac{R_{high}}{R_{low}}-1}}{Q_m}} \tag{4}$$

where Q_m is the Q factor realized by design. Q_r is the required Q factor which is defined by the impedances of antenna R_{low} and diode R_{high} (normally the diode nonlinear junction impedance) in this case. Therefore, if the diode nonlinear junction impedance is higher, it is more challenging to design a high-efficiency/low-loss matching network. It should be noted that η_m is associated with the ratio of Q_r/Q_m. Based on (4),

high-impedance antennas can be used to lessen the required Q factor of impedance matching. As one example, a high-impedance and high-Q antenna is reported in [37]. Experimental results show that such an antenna with an impedance of 80 Ω can lead to a 20 % increase in rectifying efficiency compared to a traditional 50-Ω antenna. Another design has demonstrated that with a direct conjugate matching between antenna impedance to diode impedance, the matching network can be eliminated to reduce potential insertion loss [38].

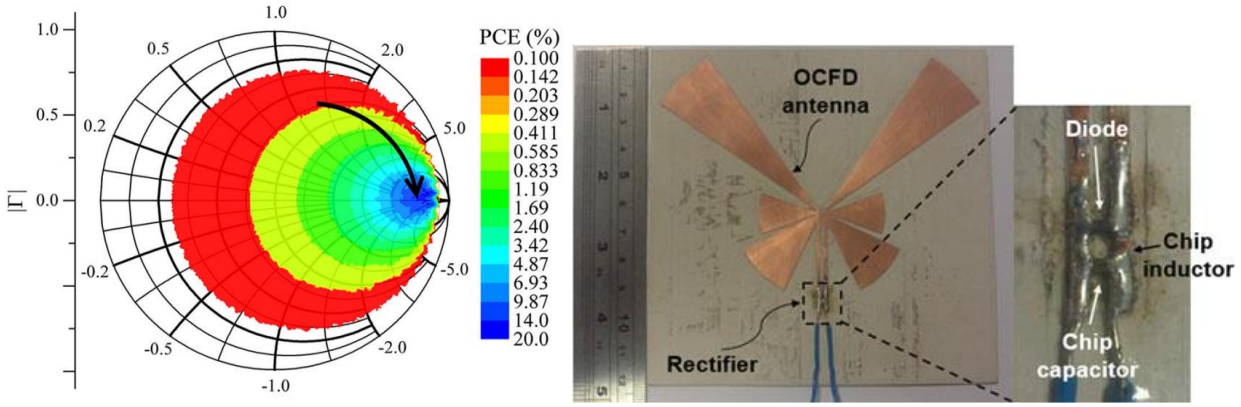

(a) (b)

Figure 11. (a) Simulated rectifying efficiency corresponding to different matching networks in the Smith chart [39]; (b) High-impedance off-center-fed dipole (OCFD) antenna realizes conjugate matching with diode directly, successfully eliminating the traditional matching network [38].

C. Load Resistance Optimization

The optimal load resistance R_{l_opt} leading to maximum rectifying efficiency can be calculated by setting the derivation of (3) to be 0. After some mathematical treatment, R_{l_opt} can be obtained as $R_j + R_s$, which equals to approximately R_j, since R_s is generally much smaller than R_j. Figure 12 has displayed diode rectifying efficiency as a function of injecting power and load resistance for diodes SMS7630 and HSMS-286x. The operating frequency is set at 880 MHz. It can be observed that the above calculated optimal load value (R_j) is only valid when the injecting power is relatively low (< −35 dBm). With a stronger injecting power, diodes SMS7630 and HSMS-286x have demonstrated different responses in terms of their optimal load resistance (Figure 12). The optimal load resistance of SMS7630 increases. In contrast,

with an opposite trend, the optimal load resistance of HSMS-286x continues to decrease at larger injecting power levels.

Optimal load resistance is of paramount importance for maximizing and maintaining the high-efficiency performance of far-field WPT rectifiers. The optimal load resistance depends on injecting RF power, and thus an optimal load tracking method is highly recommended when rectifiers are operating in a large dynamic input power range. The Maximum Power Point Tracking (MPPT) technique is widely used to ensure that optimal load resistance is connected to the rectifiers. For instance, a novel Fractional Open-Circuit Voltage Approximation (FOCVA) method was proposed to obtain the optimal load resistance in [40]. The reported rectifier shows the measured MPPT accuracy over 87 % and a wide working range from −22 dBm to −2 dBm. Another work demonstrating a larger dynamic range from −20 to 20 dBm using the MPPT method is presented in [41]. A measured peak rectifying efficiency reaches 48.19 % with respect to the input power of 0 dBm at 900 MHz.

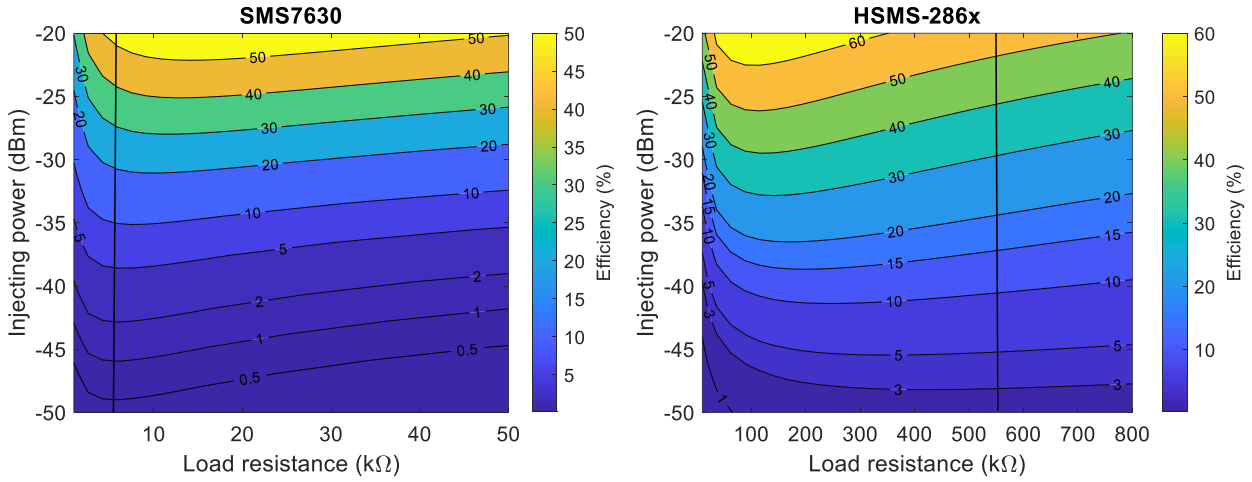

(a) (b)

Figure 12. Calculated rectifying efficiency as a function of injecting power into diode (−50 dBm to −20 dBm) and load resistance R_l for diode (a) SMS7630 and (b) HSMS-286x. Besides efficiency contours, the vertical line labels the value equivalent to $R_s + R_{j0}$, which is valid for being considered as the optimal load resistance when injecting power is relatively small.

Analysis of Diode-Based Harmonic Backscattering

When recycling ambient RF power, harmonic backscattering enhances the output of the second-harmonic component. Figure 13 (a) presents a typical circuit topology of harmonic backscattering based on a single Schottky diode [13, 42]. The quarter-wave short-circuited and open-circuited stubs are placed beside the diode to exacerbate the frequency conversion. When the fundamental signal enters the circuit, it sees the open-circuited stub as a short-circuited end due to its carefully designed length. Hence, for the fundamental signal, the equivalent circuit can be simplified in Figure 13 (b), where the diode absorbs the ambient RF injecting power. After frequency conversion from the fundamental to the second-harmonic component, the diode can be seen as a power source. At the second-harmonic frequency, the short-circuited stub stays as a short-circuited end. The equivalent circuit in Figure 13 (c) clearly explains the situation of diode acting as a second-harmonic power source. Based on this equivalent circuit analysis, the conversion efficiency from the fundamental to second-harmonic frequency can be derived as [13]:

$$\eta_c = \frac{P_{in}}{2} \cdot \left(\frac{\Re_{I0}^2}{4} + \frac{\left(\omega C_{j0} M R_{j0}\right)^2}{V_j^2} \right) \cdot \text{real}\left(\frac{Z_p^* \cdot Z_p}{Z_p^* + R_s + Z_{out}} \right) \tag{5}$$

where $\Re_{I0}$, C_{j0}, R_{j0}, M, and V_j are parameters related to the diode. M and V_j are diode grading coefficient and junction potential, respectively. Z_p and Z_{out} are the source (diode) internal impedance and output impedance, respectively. Like far-field WPT rectifier design, (5) can be used as a guideline to enhance total conversion efficiency, in other words, reduce conversion loss, by selecting suitable diode candidates.

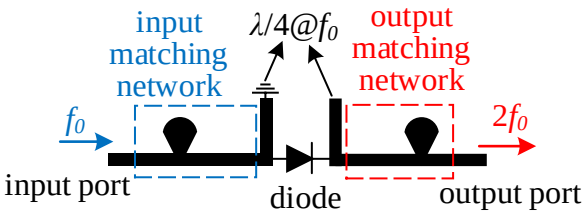

(a)

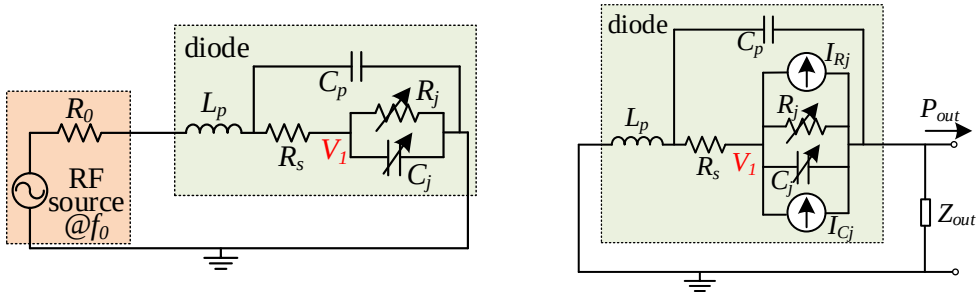

(b) (c)

Figure 13. (a) Typical circuit topology of harmonic backscattering. (b) Diode absorbs RF input power injected into the circuit. (c) Diode becomes a second-harmonic power source in the circuit.

A. Diode Selection for Harmonic Backscattering

In Table I, four diodes often used in the circuits design of harmonic backscattering are attached [42], [43]. Conversion loss results based on the ADS harmonic balance simulator are presented in Figure 14. The operating frequency is at 880 MHz, which is consistent with the above far-field WPT rectifier analysis. Figure 14 shows that SMV1430 (a varactor) is a great choice in circuit design of harmonic backscattering in a relatively low-frequency range. When the injecting power is low (−45 dBm), the conversion loss of SMV1430 is roughly 1.5 dB lower than that of its other counterparts. With the injecting power increasing to −25 dBm, the conversion loss gap between SMV1430 and HMPS-282x remains almost unchanged. Yet, on the other hand, the conversion loss of SMV1430 becomes roughly 5 dB lower than that of SMS7630 and HSMS-285x. Due to similar SPICE parameters, both conversion loss curves of SMS7630 and HSMS-285x share the same trend, similar to the analysis case of far-field WPT rectifiers discussed before.

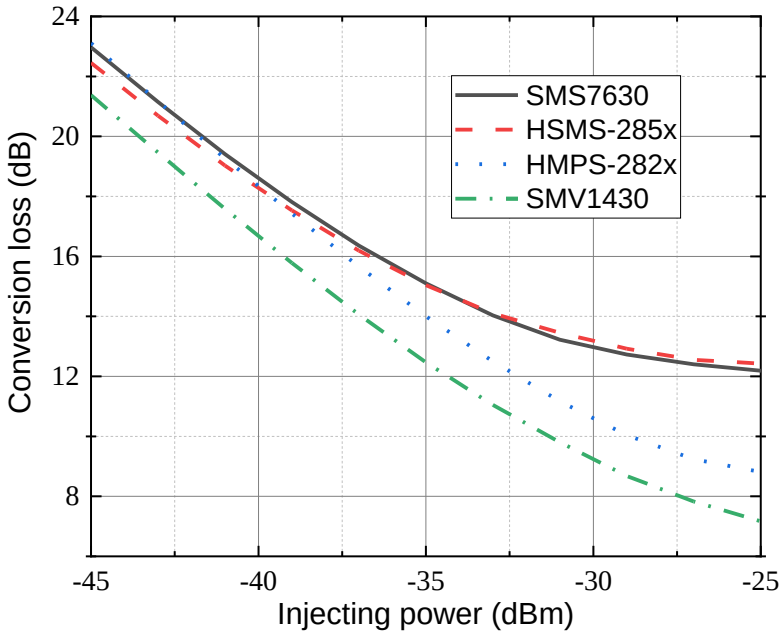

Figure 14. Conversion loss results of harmonic backscattering circuits built with four selected diodes (listed in Table I) as a function of injecting power from −45 dBm to −25 dBm.

Across the frequency band of interest (400 MHz to 2700 MHz), the conversion loss performance of harmonic backscattering circuits based on the four selected diodes is investigated. Furthermore, since diodes utilize resistive and capacitive nonlinearity simultaneously in the frequency conversion of harmonic backscattering, contributions due to nonlinear junction resistance and capacitance in the frequency conversion process are also studied. Such investigations are conducted with the aid of an analytical method reported in [13]. The corresponding results are shown in Figure 15.

For diodes SMS7630 and HSMS-285x, the influence due to operating frequency on the conversion loss is less significant than in HMPS-282x and SMV1430, which indicates that when operating frequency increases, the conversion loss of HMPS-282x and SMV1430 will degrade. For instance, the conversion loss results of HMPS-282x and SMV1430 are about 7.5 dB at – 30 dBm when the operating frequency is 880 MHz. The results degrade to roughly 25 dB at the same power level if the operating frequency increases to 2400 MHz, which means a 17.5-dB degradation due to frequency increase. Under the same conditions, the conversion loss degradation of SMS7630 and HSMS-285x are roughly 4.5 dB and 6.5 dB, respectively, when the operating frequency changes from 880 MHz to 2400 MHz. Figures 15 (f) and (h) can support

such a claim, where nonlinear junction capacitance dependent on operating frequency is dominant for diodes HMPS-282x and SMV1430 during the frequency conversion process. Hence, the conversion loss performance of the above two diodes becomes worse than SMS7630 and HSMS-285x with a higher frequency.

At a fixed operating frequency, the conversion loss of HMPS-282x and SMV1430 has smaller variations against injecting power compared to SMS7630 and HSMS-285x. This is due to different mechanisms of resistive and capacitive nonlinearity. During frequency conversion, the diode nonlinear junction resistance has by-products in the form of Joule heating. By contrast, nonlinear junction capacitance is a more efficient choice for frequency conversion without any Joule heating. Therefore, diodes SMS7630 and HSMS-285x, whose both nonlinear junction resistance and capacitance are major contributors in frequency conversion (see Figures 15 (b) and (d)), sacrifice more energy when the injecting power increases. Based on the above discussion, diodes SMS7630 and HSMS-285x are suitable for high-frequency and relatively high-power design [44]; whereas, diodes HMPS-282x and SMV1430 are good for low-frequency and low-power scenarios [45].

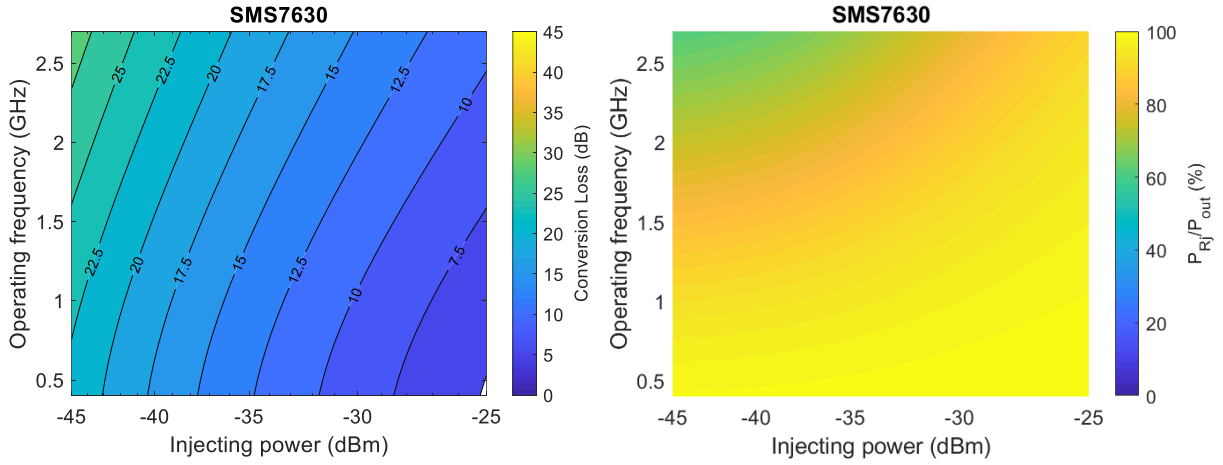

(a) (b)

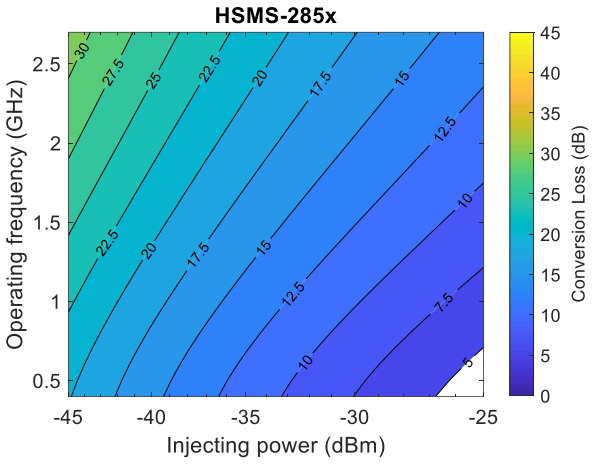
HSMS-285x
Operating frequency (GHz)
Injecting power (dBm)
Conversion Loss (dB)

(c)

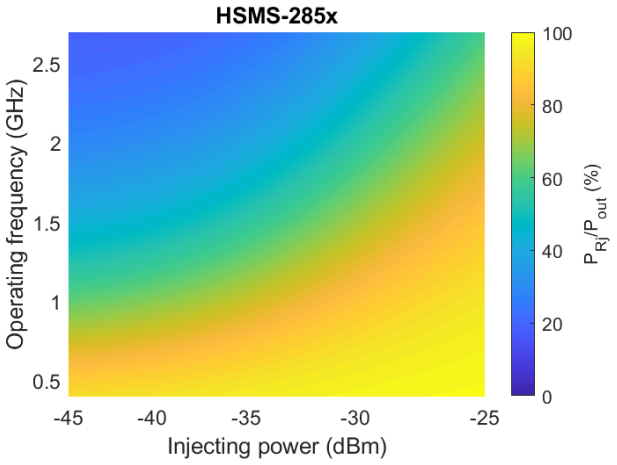
HSMS-285x
Operating frequency (GHz)
Injecting power (dBm)
P_Rj/P_out (%)

(d)

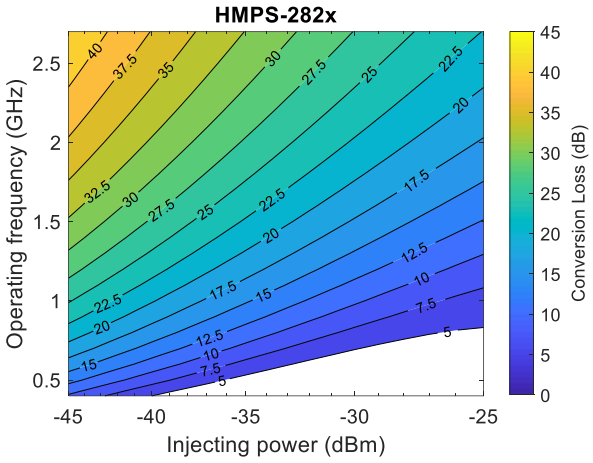
HMPS-282x
Operating frequency (GHz)
Injecting power (dBm)
Conversion Loss (dB)

(e)

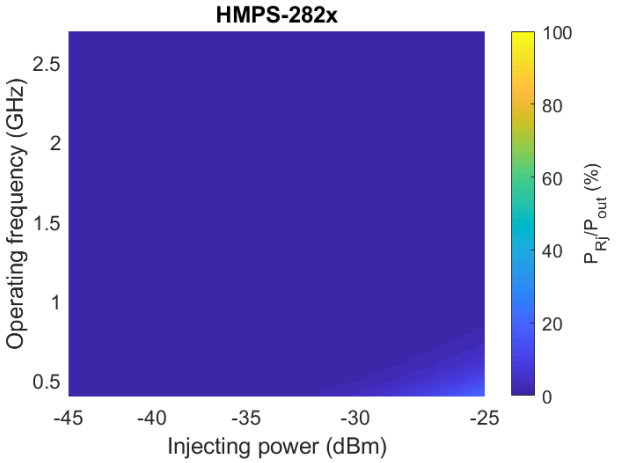
HMPS-282x
Operating frequency (GHz)
Injecting power (dBm)
P_Rj/P_out (%)

(f)

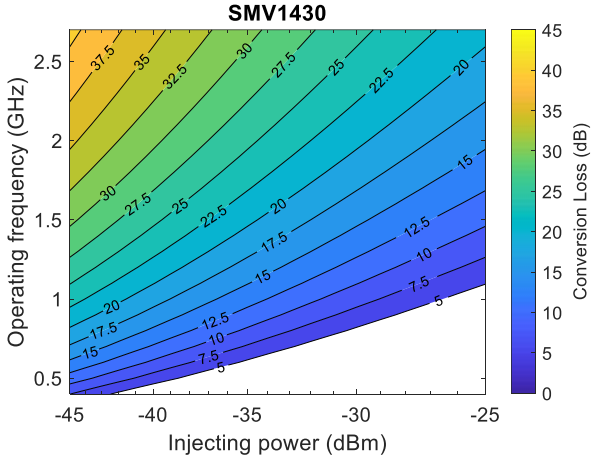
SMV1430
Operating frequency (GHz)
Injecting power (dBm)
Conversion Loss (dB)

(g)

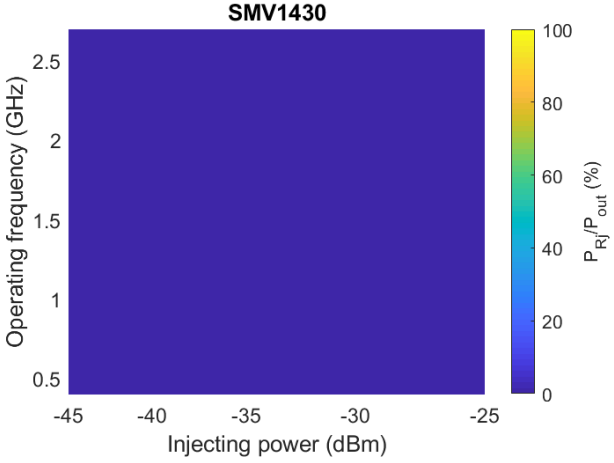
SMV1430
Operating frequency (GHz)
Injecting power (dBm)
P_Rj/P_out (%)

(h)

Figure. 15. Conversion loss and ratio of power due to resistive nonlinearity over total generated second-harmonic power as a function of operating frequency and injecting power: (a)&(b) SMS7630, (c)&(d) HSMS-2850, (e)&(f) HMPS-282x, and (g)&(h) SMV1430. Color bars are consistent for each diode.

B. Applications of Harmonic Backscattering

Harmonic backscattering has been successfully employed to detect insects and amphibians, as shown in Figure 16 [46-50]. Such applications usually feature simple loop or dipole antennas loaded with a nonlinear device to significantly reduce the total weight. Direct matching between antennas and nonlinear devices are often implemented in these designs. Impedance tuning elements are sometimes introduced for performance enhancement [51].

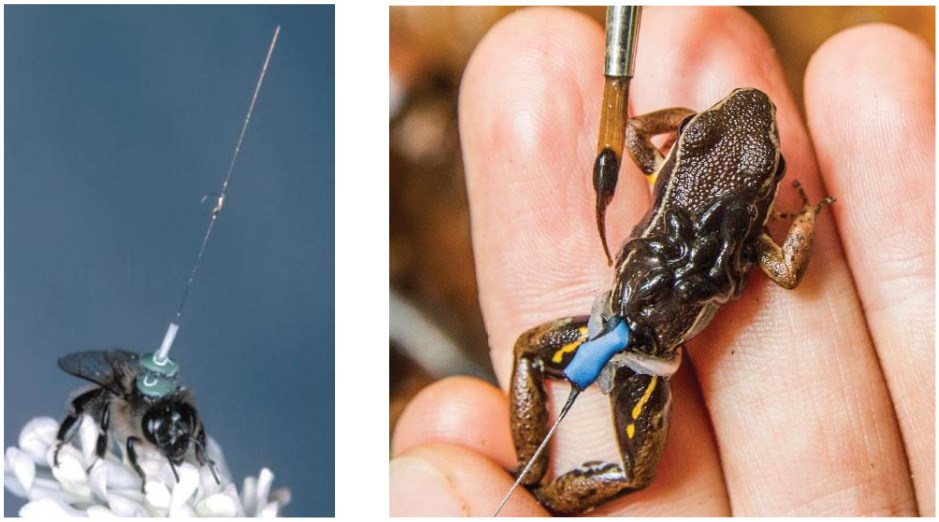

(a) (b)

Figure. 16. (a) Harmonic transponder placed on a bee for tracking its flight [46]; (b) Frog wearing a tracking transponder [48].

The above simple detection of insects and amphibians usually does not require complicated transponder/tag circuits. For other scenarios, such as structure fatigue detection, liquid sensing, and temperature sensing, certain information must be loaded into the backscattering signal. Therefore, PCB-based harmonic backscattering circuits should be carefully designed for structure fatigue detection [52], liquid sensing [53], temperature reading [54], and RECCO rescue system [55]. In these cases, useful

information is often translated into a frequency shift of the backscattering signal. Sniffer devices then decode the frequency shift and acquire real crack width, liquid, or temperature information. Figure 17 has demonstrated two application scenarios for harmonic backscattering to detect structure crack width and liquid volume.

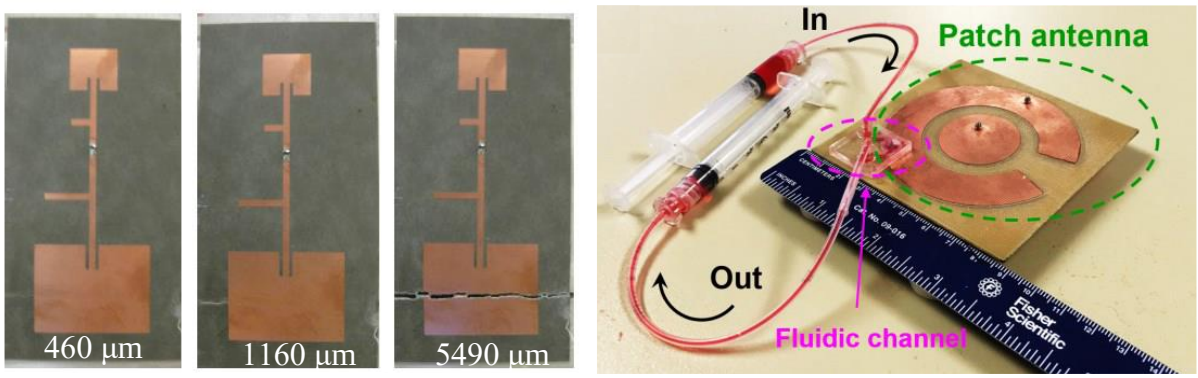

(a) (b)

Figure 17. Harmonic backscattering applied for (a) crack width [52] and (b) liquid detections [53].

Reconfigurability: Single Diode-Based Far-Field WPT and Harmonic Backscattering

As mentioned before, the primary difference between far-field WPT and harmonic backscattering is picking out the desired frequency component. It is possible to implement both functions based on one single Schottky diode for a reconfigurable and compact design. Figure 18 demonstrates such an idea, with both functions integrated on the same substrate using one Schottky diode [56]. A switch connected to the open-circuited stub near the output port is the critical component to control/select functions of either far-field WPT or harmonic backscattering. For example, if the switch is connected, the harmonic backscattering output is thus short-circuited, and the nonlinear circuit design becomes a far-field WPT rectifier. All dc output is accumulated at the load resistance. Once the switch is disconnected, this design evolves into a circuit for harmonic backscattering. Its circuit topology and equivalent circuit models are the same as those in Figure 13. Second-harmonic signals are generated and can reach the output port. Note that most of the circuit space (> 90%) of this reconfigurable design has been shared by both functions of far-field WPT and harmonic backscattering (Figure 18 (b)).

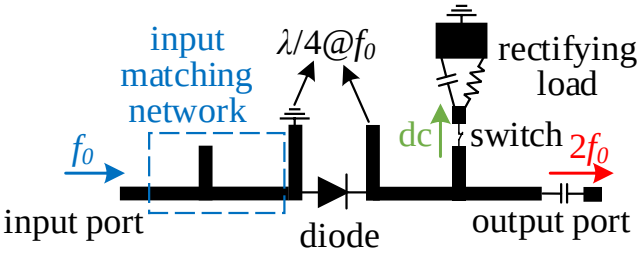

(a)

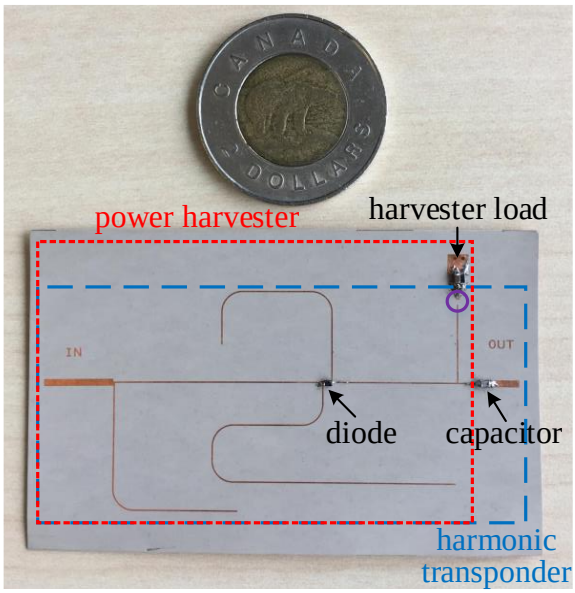

(b)

Figure 18. Reconfigurable nonlinear circuit for far-field WPT and harmonic backscattering: (a) schematic and (b) prototype.

As a preliminary design, the switch in the prototype is represented by a 0-Ω resistor. A normally-on switch is required in this design to realize function switching between far-field WPT and harmonic backscattering. For a complete design, the initial operation mode will be a far-field WPT rectifier, which enables voltage/energy collection on the load resistance. Once the load has gathered enough energy, it can trigger the switch to disconnect. Therefore, the design enters a harmonic backscattering mode and generates second-harmonic signals, which are further backscattered to sniffer devices. When power across the rectifier load goes below the switching threshold due to consumption, such a reconfigurable design will go back to the far-field WPT rectifier mode to collect power again.

Outlook

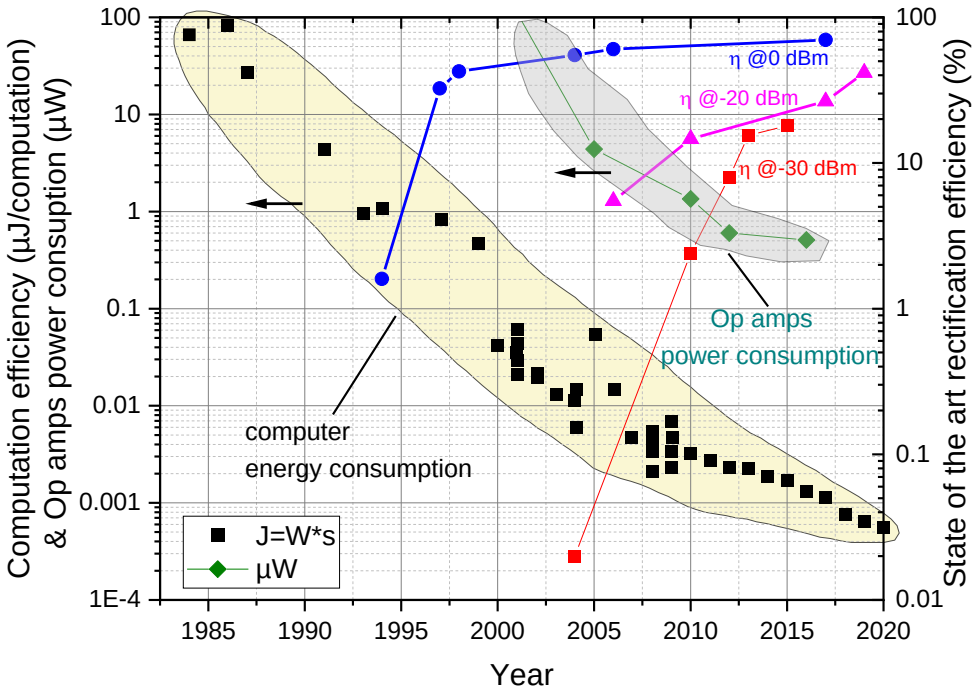

Figure 19. Evolution of the peak-output energy efficiency of computation (energy required by each computation) in the last four decades [57-59]. The energy required by the latest ultra-low-power operational amplifiers (Op amps) during one-second operation [60-63]. The rectifying efficiency of the latest far-field WPT works at input power levels of 0 dBm, −20 dBm, and −30 dB [21, 39, 64-71].

The main driving force for any new technology towards maturation are the applications. Over the past several decades, solid-state technology continued to get improved following Moore's law until the turn of the millennium [57]. Although there have been just incremental performance improvements with cutting-edge chip development in the last two decades, the peak-output energy efficiency of computation still doubles every 2.6 years [59]. The latest solid-state technology has enabled computation and operational amplifiers to work in the nanopower range, as shown in Figure 19. Meanwhile, the maturation of diode and rectifying design technology continues to drive up the efficiency of far-field WPT, especially in a power range under −20 dBm. Both evolution trends have timely bridged the gap between the low-duty, low-power electronics-based applications and the ambient RF power enabled far-field WPT. Figure 19 displays such

a historical trend. And more ambient RF powered battery-free applications are poised to emerge in the future.

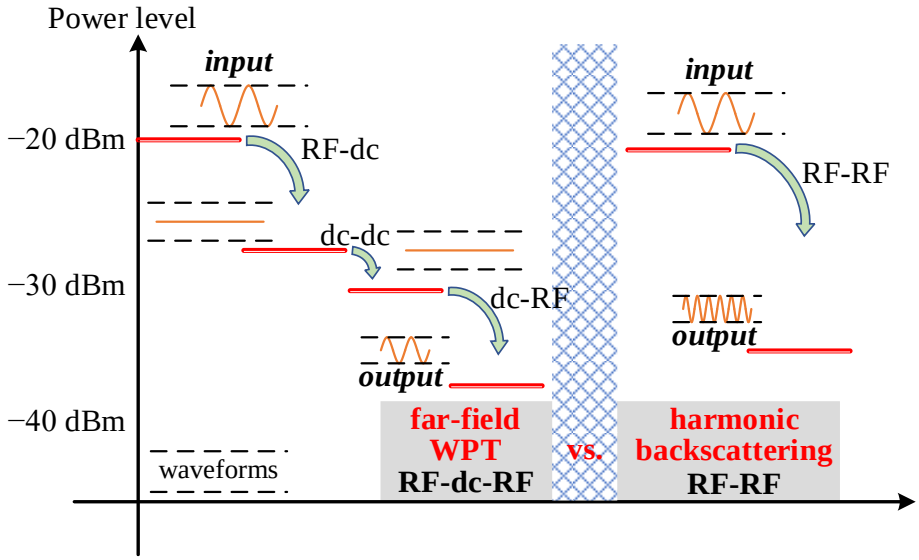

Figure 20. Comparisons of power budget and waveform change between far-field WPT and harmonic backscattering used in applications.

As for the harmonic backscattering, this may be a more power-efficient solution for certain applications compared to the far-field WPT. Figure 20 presents the differences in power budget and waveform change between far-field WPT and harmonic backscattering used in applications. Far-field WPT converts an incident sinusoidal wave into dc through the rectifying process first. If the input power is −20 dBm, such RF-dc conversion efficiency can reach roughly 20 % [21]. Then, to enable specific applications, the rectified dc voltage usually needs to be amplified, which requires a dc-dc step-up converter. Based on recent works [72], this dc-dc conversion efficiency is estimated as 50 % at a low-power level. Finally, an integrated voltage-controlled oscillator (VCO) featuring low power and low phase noise is the critical component for realizing communications. The dc-RF conversion efficiency of such VCOs are normally low: 17.5 % is our estimation here [73]. For far-field WPT, the entire process of RF-dc-RF conversion has been shown in Figure 20, where the power budget estimation and waveform change are also included. By contrast, the harmonic backscattering shows a relatively simple conversion, i.e., fundamental RF to its second harmonic (RF-RF). Compared to the far-field WPT, the final power loss of harmonic backscattering

would be smaller if the input power is −20 dBm [13]. It is worth noting that the power budget shown in Figure 20 is a rough estimation, as they depend on specific applications. Far-field WPT can support more complicated tasks at the cost of larger power consumption. Whereas, less power-hungry harmonic backscattering is more suitable to handle simple applications. Indeed, the superior solution will be a proper reconfigurable design with two functions integrated for scavenging ambient RF energy more efficiently.

Acknowledgement

This work is financially supported by the Natural Science Engineering Research Council of Canada (NSERC). The authors would like to express gratitude to the technical supporting team of Poly-GRAMES Research Center, Polytechnique Montreal, for their fabrication and measurement help.

References

[1] J. H. Bryant, "The first century of microwaves-1886 to 1986," *IEEE Trans. Microw. Theory Techn.,* vol. 36, no. 5, pp. 830-858, May 1988.

[2] K. Wu, D. Choudhury, and H. Matsumoto, "Wireless power transmission, technology, and applications," *Proc. IEEE*, vol. 101, no. 6, pp. 1271-1275, Jun. 2013.

[3] C. H. P. Lorenz, S. Hemour, and K. Wu, "Physical mechanism and theoretical foundation of ambient RF power harvesting using zero-bias diodes," *IEEE Trans. Microw. Theory Techn.,* vol. 64, no. 7, pp. 2146-2158, Jul. 2016.

[4] Z. Popovic, "Cut the cord: Low-power far-field wireless powering," *IEEE Microw. Mag.,* vol. 14, no. 2, pp. 55-62, Mar./Apr. 2013.

[5] U. Muncuk, K. Alemdar, J. D. Sarode, and K. R. Chowdhury, "Multiband ambient RF energy harvesting circuit design for enabling batteryless sensors and IoT," *IEEE Internet Things J.*,vol. 5, no. 4, pp. 2700-2714, Aug. 2018.

[6] T. Imai *et al.*, "Development of high frequency band over 6 GHz for 5G mobile communication systems," in *Proc. 9th Eur. Conf. Antennas Propag.*, Lisbon, Portugal, Apr. 2015, pp. 1-4.

[7] M. Pinuela, P. D. Mitcheson, and S. Lucyszyn, "Ambient RF energy harvesting in urban and semi-urban environments," *IEEE Trans. Microw. Theory Techn.,* vol. 61, no. 7, pp. 2715-2726, Jul. 2013.

[8] H. Takhedmit, "Ambient RF power harvesting: Application to remote supply of a batteryless temperature sensor," in *Proc. IEEE Int. Smart Cities Conf.*, Trento, Italy, Sept. 2016, pp. 1-4.

[9] O. M. AbdelGhany, A. G. Sobih, and A. M. El-Tager, "Outdoor RF spectral study available from cell-phone towers in sub-urban areas for ambient RF energy harvesting," *IOP Conf. Ser.: Mater. Sci. Eng.*, vol. 610, p. 012086, 2019.

[10] X. Gu, L. Grauwin, D. Dousset, S. Hemour, and K. Wu, "Dynamic ambient RF energy mapping of Montreal for battery-free IoT sensor network planning," Submitted.

[11] S. Kim *et al.*, "Ambient RF energy-harvesting technologies for self-sustainable standalone wireless sensor platforms," *Proc. IEEE,* vol. 102, no. 11, pp. 1649-1666, Nov. 2014.

[12] J. Kimionis *et al.*, "Zero-power sensors for smart objects: Novel zero-power additively manufactured wireless sensor modules for IoT applications," *IEEE Microw. Mag.*, vol. 19, no. 6, pp. 32-47, Sept./Oct. 2018.

[13] X. Gu, N. N. Srinaga, L. Guo, S. Hemour, and K. Wu, "Diplexer-Based Fully Passive Harmonic Transponder for Sub-6-GHz 5G-Compatible IoT Applications," *IEEE Trans. Microw. Theory Techn.,* vol. 67, no. 5, pp. 1675-1687, May 2019.

[14] T.-H. Lin *et al.*, "On-body long-range wireless backscattering sensing system using inkjet-/3-D-printed flexible ambient rf energy harvesters capable of simultaneous dc and harmonics generation," vol. 65, no. 12, pp. 5389-5400, Dec. 2017.

[15] F. Amato and S. Hemour, "The Harmonic Tunneling Tag: a Dual-Band Approach to Backscattering Communications," in *Proc. IEEE Int. Conf. RFID Technol. Appl.*, Pisa, Italy, Sept. 2019, pp. 244-247.

[16] H. C. Torrey, C. Austin, and S. A. Goudsmit, *Crystal Rectifiers*, New York, NY, USA: McGraw-Hill, 1948.

[17] S. Hemour and K. Wu, "Radio-frequency rectifier for electromagnetic energy harvesting: Development path and future outlook," *Proc. IEEE,* vol. 102, no. 11, pp. 1667-1691, Nov. 2014.

[18] S. Hemour *et al.*, "Towards low-power high-efficiency RF and microwave energy harvesting," *IEEE Trans. Microw. Theory Techn.,* vol. 62, no. 4, pp. 965-976, Apr. 2014.

[19] W. Shockley, "The Theory of p-n Junctions in Semiconductors and p-n Junction Transistors," *Bell Sys. Tech. J.,* vol. 28, no. 3, pp. 435-489, Jul. 1949.
[20] S. Hemour, X. Gu, and K. Wu, "Efficiency of Rectenna," in *Recent Wireless Power Transfer Technologies via Radio Waves,* N. Shinohara, Ed., ed: River Publishers, 2018, pp. 95-132.
[21] X. Gu, L. Guo, S. Hemour, and K. Wu, "Optimum temperatures for enhanced power conversion efficiency (PCE) of zero bias diode-based rectifiers," *IEEE Trans. Microw. Theory Techn.,* to be published.
[22] V. Palazzi *et al.*, "A novel ultra-lightweight multiband rectenna on paper for RF energy harvesting in the next generation LTE bands," *IEEE Trans. Microw. Theory Tech.,* vol. 66, no. 1, pp. 366-379, Jan. 2018.
[23] S. Shen, Y. Zhang, C.-Y. Chiu, and R. Murch, "A Triple-band High-Gain Multibeam Ambient RF Energy Harvesting System Utilizing Hybrid Combining," *IEEE Trans. Ind. Electron.*, vol. 67, no. 11, pp. 9215-9226, Nov. 2020.
[24] C.-Y. Hsu, S.-C. Lin, and Z.-M. Tsai, "Quadband rectifier using resonant matching networks for enhanced harvesting capability," *IEEE Microw. Wireless Compon. Lett.,* vol. 27, no. 7, pp. 669-671, Jul. 2017.
[25] V. Kuhn, C. Lahuec, F. Seguin, and C. Person, "A multi-band stacked RF energy harvester with RF-to-DC efficiency up to 84%," *IEEE Trans. Microw. Theory Techn.,* vol. 63, no. 5, pp. 1768-1778, May 2015.
[26] H. Sun, Y.-X. Guo, M. He, and Z. Zhong, "A dual-band rectenna using broadband Yagi antenna array for ambient RF power harvesting," *IEEE Antennas Wireless Propag. Lett.*, vol. 12, pp. 918-921, Jul. 2013.
[27] U. Olgun, C.-C. Chen, and J. Volakis, "Investigation of rectenna array configurations for enhanced RF power harvesting," *IEEE Antennas Wireless Propag. Lett.*, vol. 10, pp. 262-265, Apr. 2011.
[28] E. Vandelle, T.-P. Vuong, G. Ardila, K. Wu, and S. Hemour, "Harvesting Ambient RF Energy Efficiently With Optimal Angular Coverage," *IEEE Trans. Antennas Propag.,* vol. 67, no. 3, pp. 1862-1873, Mar. 2019.
[29] H. Sun and W. Geyi, "A new rectenna using beamwidth-enhanced antenna array for RF power harvesting applications," *IEEE Antennas Wireless Propag. Lett.,* vol. 16, pp. 1451-1454, Dec. 2016.
[30] Y.-Y. Hu, S. Sun, H. Xu, and H. Sun, "Grid-Array Rectenna With Wide Angle Coverage for Effectively Harvesting RF Energy of Low Power Density," *IEEE Trans. Microw. Theory Techn.,* vol. 67, no. 1, pp. 402-413, Jan. 2019.
[31] W. Brown and J. Triner, "Experimental thin-film, etched-circuit rectenna," in *Proc. IEEE MTT-S Int. Microw. Symp. Dig.,* Dallas, TX, USA, Jun. 1982, pp. 185-187.
[32] X. Gu *et al.*, "Hybridization of Integrated Microwave and Mechanical Power Harvester," *IEEE Access,* vol. 6, pp. 13921-13930, Mar. 2018.
[33] L. Guo, X. Gu, P. Chu, S. Hemour, and K. Wu, "Collaboratively Harvesting Ambient Radiofrequency and Thermal Energy," *IEEE Trans. Ind. Electron.,* vol. 67, no. 5, May 2020.
[34] K. Niotaki, A. Collado, A. Georgiadis, S. Kim, and M. M. Tentzeris, "Solar/electromagnetic energy harvesting and wireless power transmission," *Proc. IEEE,* vol. 102, no. 11, pp. 1712-1722, Nov. 2014.
[35] X. Gu, S. Hemour, and K. Wu, "Enabling Far-Field Ambient Energy Harvesting Through Multi-Physical Sources," in *Proc. Asia-Pac. Microw. Conf.*, Kyoto, Japan, Nov. 2018, pp. 204-206.
[36] X. Gu, S. Hemour, L. Guo, and K. Wu, "Integrated Cooperative Ambient Power Harvester Collecting Ubiquitous Radio Frequency and Kinetic Energy," *IEEE Trans. Microw. Theory Techn.,* vol. 66, no. 9, pp. 4178-4190, Sept. 2018.
[37] N. Shinohara and Y. Zhou, "Development of rectenna with high impedance and high Q antenna," in *Proc. Asia-Pac. Microw. Conf.*, Sendai, Japan, Nov. 2014, pp. 600-602.
[38] C. Song *et al.*, "Matching network elimination in broadband rectennas for high-efficiency wireless power transfer and energy harvesting," *IEEE Trans. Ind. Electron.,* vol. 64, no. 5, pp. 3950-3961, May 2017.
[39] C. H. P. Lorenz *et al.*, "Breaking the Efficiency Barrier for Ambient Microwave Power Harvesting With Heterojunction Backward Tunnel Diodes," *IEEE Trans. Microw. Theory Techn.,* vol. 63, no. 12, pp. 4544-4555, Dec. 2015.
[40] Z. Zeng, J. J. Estrada-López, M. A. Abouzied, and E. Sánchez-Sinencio, "A Reconfigurable Rectifier with Optimal Loading Point Determination for RF Energy Harvesting from-22 dBm to-2 dBm," *IEEE Trans. Circuits Syst. II Exp. Briefs,* vol. 67, no. 1, pp. 87-91, Jan. 2019.
[41] S.-Y. Kim *et al.*, "A-20 to 30 dBm Input Power Range Wireless Power System with a MPPT-based Reconfigurable 48% Efficient RF Energy Harvester and 82% Efficient A4WP Wireless Power Receiver with Open Loop Delay Compensation," *IEEE Trans. Power Electron.,* vol. 34, no. 7, pp. 6803-6817, Jul. 2019.
[42] X. Gu, L. Guo, S. Hemour, and K. Wu, "Novel diplexer-based harmonic transponder for 5G-compatible IoT applications," in *Proc. IEEE MTT-S Wireless Power Transf. Conf.*, Montreal, Canada, Jun. 2018, pp. 1-4.
[43] K. Rasilainen, J. Ilvonen, A. Lehtovuori, J.-M. Hannula, and V. Viikari, "On design and evaluation of harmonic transponders," *IEEE Trans. Antennas Propag.,* vol. 63, no. 1, pp. 15-23, Jan. 2015.
[44] X. Gu, L. Guo, S. Hemour, and K. Wu, "Analysis and Exploitation of Diplexer-based Fully Passive Harmonic Transponder for 5G Applications," in *Proc. IEEE MTT-S Int. Microw. Workshop Ser. 5G Hardw. Syst. Technol.*, Dublin, Ireland, Aug. 2018, pp. 1-3.
[45] K. Rasilainen, J. Ilvonen, J.-M. Hannula, and V. Viikari, "Designing Harmonic Transponders Using Lumped-Component Matching Circuits," *IEEE Antennas Wireless Propag. Lett.,* vol. 16, pp. 246-249, May 2016.
[46] E. A. Capaldi *et al.*, "Ontogeny of orientation flight in the honeybee revealed by harmonic radar," *Nature*, vol. 403, no. 6769, pp. 537-540, Feb. 2000.
[47] A. Lavrenko, B. Litchfield, G. Woodward, and S. Pawson, "Design and evaluation of a compact harmonic transponder for insect tracking," *IEEE Microw. Wireless Compon. Lett.*, vol. 30, no. 4, pp. 445-448, Apr. 2020.
[48] A. Pašukonis, K. B. Beck, M.-T. Fischer, S. Weinlein, S. Stückler, and E. Ringler, "Induced parental care in a poison frog:

a tadpole cross-fostering experiment," *J. Exp. Biol.*, vol. 220, no. 21, pp. 3949-3954, Aug. 2017.
[49] T. Langkilde and R. A. Alford, "The tail wags the frog: harmonic radar transponders affect movement behavior in Litoria lesueuri," *J. Herpetol.*, vol. 36, no. 4, pp. 711-715, Dec. 2002.
[50] B. G. Colpitts, and G. Boiteau, "Harmonic radar transceiver design: miniature tags for insect tracking," *IEEE Trans. Antennas Propag.*, vol. 52, no. 11, pp. 2825-2832, Nov. 2004.
[51] R. Brazee, E. Miller, M. Reding, M. Klein, B. Nudd, and H. Zhu, "A transponder for harmonic radar tracking of the black vine weevil in behavioral research," *Trans. Amer. Soc. Agricultural Eng.*, vol. 48, no. 2, pp. 831-838, Feb. 2005.
[52] C. Cho, X. Yi, D. Li, Y. Wang, and M. Tentzeris, "Passive wireless frequency doubling antenna sensor for strain and crack sensing," *IEEE Sensors J.*, vol. 16, no. 14, pp. 5725-5733, Jul. 2016.
[53] L. Zhu, M. Farhat, Y.-C. Chen, K. N. Salama, and P.-Y. Chen, "A Compact, Passive Frequency-Hopping Harmonic Sensor Based on a Microfluidic Reconfigurable Dual-Band Antenna," *IEEE Sensors J.*, to be published.
[54] X. Gu, S. Hemour, and K. Wu, "Remote Temperature Sensing Based on Battery-Free Harmonic Backscattering," in *Proc. IEEE Int. Symp. Antennas Propag. USNC-URSI Radio Sci. Meeting*, Montreal, Canada, Jul. 2020, pp. 1-2.
[55] S. Zorn, R. Rose, A. Goetz, and R. Weigel, "A novel technique for mobile phone localization for search and rescue applications," in *Proc. IEEE Int. Conf. Indoor Positioning Indoor Navigat.*, Zurich, Switzerland, Sept. 2010, pp. 1-4.
[56] X. Gu, S. Hemour, and K. Wu, "Reconfigurable Nonlinear Circuit for Wireless Power Harvesting and Backscattering," in *Proc. 49th Eur. Microw. Conf.*, Paris, France, Oct. 2019, pp. 543-546.
[57] J. Koomey, S. Berard, M. Sanchez, and H. Wong, "Implications of historical trends in the electrical efficiency of computing," *IEEE Ann. History Comput.*, vol. 33, no. 3, pp. 46-54, Mar. 2011.
[58] J. Koomey and S. Naffziger, "Moore's Law might be slowing down, but not energy efficiency," *IEEE Spectrum*, vol. 52, no. 4, p. 35, Mar. 2015.
[59] J. Koomey and S. Naffziger, "Energy efficiency of computing: what's next," Accessed on Nov. 28, 2016. [Online]. Available: https://cdn.baseplatform.io/files/base/ebm/electronicdesign/document/2019/03/electronicdesign_10815_energyefficiencyofcomputingwhatsnext.pdf
[60] Texas Instruments, "LPV511 Micropower, Rail-to-Rail Input and Output Operational Amplifier," LPV511 datasheet, 2005, [Online]. Available: http://www.ti.com/product/LPV511
[61] Touchstone Semiconductor. "TS1002-04 0.8V/0.6µA Rail-to-Rail Dual/Quad Op Amps," TS1002 datasheet, 2010, [Online]. Available: https://www.silabs.com/documents/public/data-sheets/TS1002-04.pdf
[62] Maxim Intgrated. "MAX44264 nanoPower Op Amp in a Tiny 6-Bump WLP," MAX44264 datasheet, 2010, [Online]. Available: https://www.maximintegrated.com/en/products/analog/amplifiers/MAX44264.html
[63] Texas Instruments. "LPV802 Single Channel 450nA Nanopower Operational Amplifier," LPV802 datasheet, 2016, [Online]. Available: http://www.ti.com/product/LPV801
[64] H. Nakamoto *et al.*, "A passive UHF RFID tag LSI with 36.6% efficiency CMOS-only rectifier and current-mode demodulator in 0.35 um FeRAM technology," in *Proc. IEEE Int. Solid-State Circuits Conf. Dig. Tech. Papers*, San Francisco, CA, USA, Feb. 2006, pp. 1201-1210.
[65] C. Meneses Ghiglino, "Ultra-Wideband (UWB) rectenna design for Electromagnetic Energy Harvesting," Masters thesis, Dept. Teoria del Senyali Comun., Escola Tecnica Superior d'Enginyeria de Telecomun. de Barcelona, Catalunya, Spain, 2010.
[66] C. Song, Y. Huang, J. Zhou, and P. Carter, "Improved ultrawideband rectennas using hybrid resistance compression technique," *IEEE Trans. Antennas Propag.,* vol. 65, no. 4, pp. 2057-2062, Apr. 2017.
[67] J. O. McSpadden, L. Fan, and K. Chang, "Design and experiments of a high-conversion-efficiency 5.8-GHz rectenna," *IEEE Trans. Microw. Theory Techn.,* vol. 46, no. 12, pp. 2053-2060, Dec. 1998.
[68] J. O. McSpadden, L. Fan, and K. Chang, "A high conversion efficiency 5.8 GHz rectenna," in *Proc. IEEE MTT-S Int. Microw. Symp. Dig.*, Denver, CO, USA, Jun. 1997, pp. 547-550.
[69] J. O. McSpadden and K. Chang, "A dual polarized circular patch rectifying antenna at 2.45 GHz for microwave power conversion and detection," in *Proc. IEEE MTT-S Int. Microw. Symp. Dig.*, San Diego, CA, USA, May 1994, pp. 1749-1752.
[70] J. A. Hagerty, F. B. Helmbrecht, W. H. McCalpin, R. Zane, and Z. B. Popović, "Recycling ambient microwave energy with broad-band rectenna arrays," *IEEE Trans. Microw. Theory Techn.,* vol. 52, no. 3, pp. 1014-1024, Mar. 2004.
[71] Y.-J. Ren and K. Chang, "5.8-GHz circularly polarized dual-diode rectenna and rectenna array for microwave power transmission," *IEEE Trans. Microw. Theory Techn.,* vol. 54, no. 4, pp. 1495-1502, Apr. 2006.
[72] T. Ozaki, T. Hirose, H. Asano, N. Kuroki, and M. Numa, "Fully-integrated high-conversion-ratio dual-output voltage boost converter with MPPT for low-voltage energy harvesting," *IEEE J. Solid-State Circuits*, vol. 51, no. 10, pp. 2398-2407, Oct. 2016.
[73] C. Li and A. Liscidini, "Class-C PA-VCO Cell for FSK and GFSK Transmitters," *IEEE J. Solid-State Circuits*, vol. 51, no. 7, pp. 1537-1546, Jul. 2016.